Slingsby, C. V. Robinson, *Proc. Natl. Acad. Sci. U.S.A.* **100**, 10611 (2003).
31. E. H. J. Koch, P. Vachette, D. I. Svergun, *Q. Rev. Biophys.* **36**, 147 (2003).
32. P. Aloy *et al.*, *Science* **303**, 2026 (2004).
33. We thank P. Gollnick for the TRAP protein complex used in these studies as well as M. Vendruscolo and M. McCammon for helpful discussions. This work is supported through the Walters-Kundert Trust and the Research Councils' Basic Technology Programme.

Supporting Online Material
www.sciencemag.org/cgi/content/full/1120177/DC1
Materials and Methods
SOM Text
Figs. S1 to S6
Table S1
References and Notes

14 September 2005; accepted 31 October 2005
Published online 17 November 2005;
10.1126/science.1120177
Include this information when citing this paper.

Rapid Chiral Assembly of Rigid DNA Building Blocks for Molecular Nanofabrication

R. P. Goodman,[1] I. A. T. Schaap,[2] C. F. Tardin,[2] C. M. Erben,[1] R. M. Berry,[1] C. F. Schmidt,[2] A. J. Turberfield[1]*

Practical components for three-dimensional molecular nanofabrication must be simple to produce, stereopure, rigid, and adaptable. We report a family of DNA tetrahedra, less than 10 nanometers on a side, that can self-assemble in seconds with near-quantitative yield of one diastereomer. They can be connected by programmable DNA linkers. Their triangulated architecture confers structural stability; by compressing a DNA tetrahedron with an atomic force microscope, we have measured the axial compressibility of DNA and observed the buckling of the double helix under high loads.

Three-dimensional (3D) construction by self-assembly requires rigid building blocks such as tetrahedra. DNA is an ideal material for nanofabrication of rigid structures because assembly can be controlled by base-pairing (*1*) and is relatively inexpensive and simple to execute (*2*). However, DNA nanofabrication presents the problem of avoiding unwanted by-products. It is often possible to ensure that the target structure is the one that creates the largest number of Watson-Crick base pairs and is therefore the most stable product. Usually, however, there are many other possible structures that are only slightly less stable. If all component oligonucleotides are simply mixed without precaution, the yield of the target structure can be extremely low, and disordered polymeric structures can form instead. Successful strategies for the synthesis of 2D periodic structures involve a hierarchy of interactions in which preformed building blocks are linked by weaker interactions to form an array (*3*–*5*), but 3D construction is much less well developed.

Polyhedral DNA nanostructures with the connectivities of a cube (*6*) and of truncated and regular octahedra (*7*, *8*) have been made, each using a different synthetic strategy. Trisoligonucleotidyls—three oligonucleotides connected by a trifunctional linker (*9*)—have also been reported to form tetrahedra (*10*). The cube (*6*) was assembled in solution by ligation of 10 oligonucleotides, in three stages with intermediate purification steps, with 1% yield. The solid-support synthesis of the truncated octahedron (*7*) allowed greater control of the assembly process: Two halves of an edge could be joined by ligation only after a deprotection step in which a restriction endonuclease was used to cleave two precursor hairpin loops to create overlapping sticky ends. This synthesis, starting with 48 oligonucleotides, took approximately two worker-years; yield was less than 1%. Both the cube and the truncated octahedron were covalently closed catenanes that could not be disassembled without breaking covalent bonds: In designing the octahedron (*8*), this robust design principle was sacrificed to permit assembly by folding. The principal component of the octahedron, a 1.7-kb oligonucleotide synthesized using 64 synthetic oligonucleotides and amplified by cloning, was designed to have branched secondary structure; the octahedron was formed when branches folded and were bound together by intramolecular paranemic interactions (*11*).

The junctions that form the vertices of these 3D nanostructures are flexible. DNA nanostructures with triangulated architectures may be capable of resisting deformation, but their mechanical properties have not been measured. Rigidity is not enough to ensure that a DNA polyhedron has a robust and well-defined structure; it is also necessary to select one of the two possible diastereomers (enantiomers with respect to the identities of their vertices) that satisfy the pattern of connectivity imposed by the design of hybridization interactions. Discrimination between diastereomers of DNA polyhedra has yet to be demonstrated, and the stereoselectivity of the syntheses described above is unknown.

We have synthesized a family of DNA tetrahedra that have been designed to self-assemble in a single step in only a few seconds. A single diastereomer can be synthesized with yields as high as 95%. We demonstrate their versatility as building blocks for 3D nanofabrication by assembling one regular and nine different irregular tetrahedra and by connecting them with programmable DNA linkers. We then use atomic force microscopy (AFM) to image the tertiary structure of individual tetrahedra and to demonstrate their rigidity, which we exploit to measure the response of DNA to axial compression.

The DNA tetrahedron is designed to be mechanically robust; it consists of rigid triangles of DNA helices covalently joined at the vertices (Fig. 1A) (*12*). The four component oligonucleotides each run around one face and hybridize to form the double-helical edges. Four edges contain nicks (i.e., breaks in the DNA backbone) where the 5′ and 3′ ends of an oligonucleotide meet. At each vertex, adjacent edges are attached through single, unpaired "hinge" bases. In contrast to the challenging syntheses of DNA cubes (*6*) and octahedra (*7*, *8*), the synthesis of tetrahedra is extremely simple: All four oligonucleotides are combined in equimolar quantities in hybridization buffer at 95°C and then cooled to 4°C in 30 s (*13*).

Tetrahedra form with ~95% yield and migrate as single bands on a nondenaturing electrophoresis gel (fig. S1) (*13*). A covalently closed catenane may be produced by enzymatic ligation of the four nicks in the DNA backbone. We believe that the designed hierarchy of interactions between oligonucleotides contributes to the high efficiency of this one-step synthesis. We expect hybridization between oligonucleotides 1 and 2, and also 3 and 4, to form the stable, unnicked edges B and E (Fig. 1A) to occur first as the solution temperature falls. Other edges can then form cooperatively; once the formation of any other edge has linked these pairs to form a four-strand complex, all further hybridization interactions required to

[1]Clarendon Laboratory, Department of Physics, University of Oxford, Parks Road, Oxford OX1 3PU, UK. [2]Department of Physics and Astronomy, de Boelelaan 1081, Vrije Universiteit, 1081 H Amsterdam, Netherlands.

*To whom correspondence should be addressed. E-mail: a.turberfield@physics.ox.ac.uk

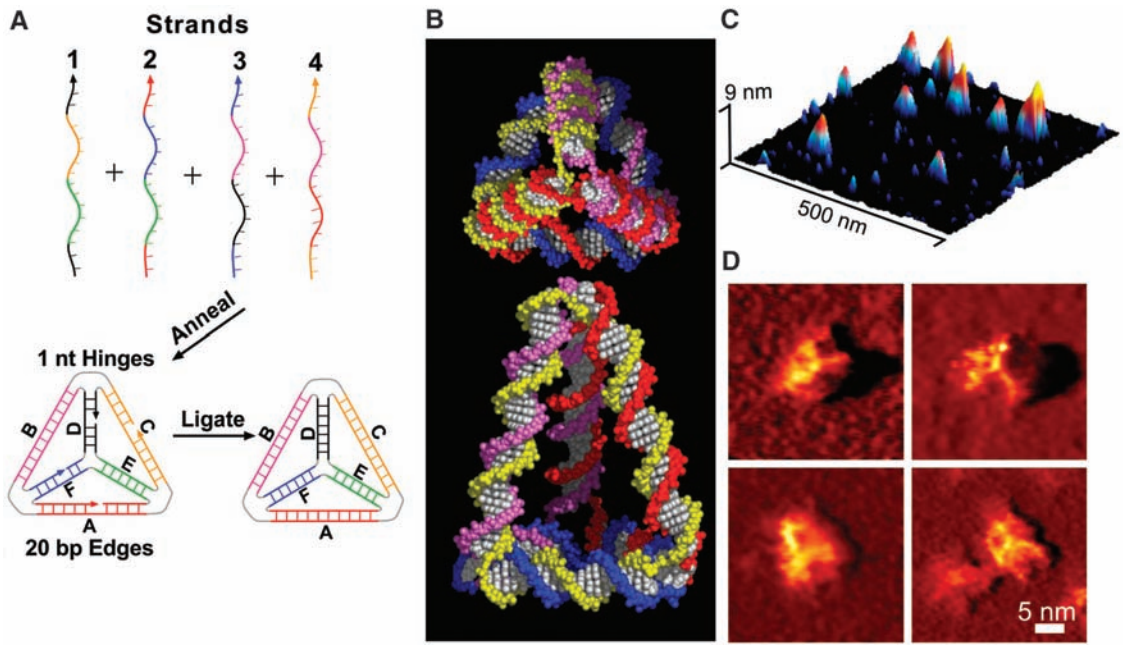

Fig. 1. DNA tetrahedra. (**A**) Design of a DNA tetrahedron formed by annealing four oligonucleotides. Complementary subsequences that hybridize to form each edge are identified by color. (**B**) Two views of a space-filling representation of a 3×20/3×30-bp tetrahedron. The backbone of each oligonucleotide is indicated by a single color. (**C**) AFM image showing several tetrahedra on a mica surface. (**D**) AFM images, recorded with ultrasharp tips, of four tetrahedra; the three upper edges are resolved.

complete the tetrahedron are intramolecular and are therefore expected to be faster than competing intermolecular interactions that would form larger complexes. The positions of the nicks are such that none of these intramolecular interactions is substantially hindered by bonds already formed.

The tetrahedra imaged by AFM in Fig. 1, C and D, were designed to have three 30–base pair (bp) edges meeting at one vertex and three 20-bp edges bounding the opposite face (a molecular model is shown in Fig. 1B). They are expected to bind to a surface in one of two orientations, with heights of ~10.5 nm if resting on the small face and ~7.5 nm if resting on any of the other three faces. Figure 1C, recorded with a tip 20 nm in radius, shows several objects with heights consistent with the two orientations. Figure 1D shows high-resolution images, obtained using ultrasharp tips with radii of only 2 to 3 nm, that resolve the three upper edges of individual tetrahedra.

To confirm that our constructs had the topology of a tetrahedron, we used selective enzymatic ligation and digestion. Incubation with T4 DNA ligase leads to ligation (covalent closure) of the nicks where the 5′ and 3′ ends of an oligonucleotide are held together in the middle of an edge, but only if the 5′ end is prepared with a terminal phosphate group. Sixteen regular 20-bp tetrahedra were formed with every combination of ligated and unligated nicks. In the denaturing gels shown in Fig. 2, A to C, linear oligonucleotides dissociated and only circular, catenated oligonucleotides were constrained to migrate together. According to the design, each ligation should produce a circular oligonucleotide and all circles produced by multiple ligations should be catenated with a linking number corresponding to the number of complete helical turns in each edge—in this case, two. The expected bands appeared when one, two, three, and four oligonucleotides were ligated (products of failed ligation were also observed). Digestion with exonuclease III, which can hydrolyze duplex DNA from a free 3′ end, confirmed

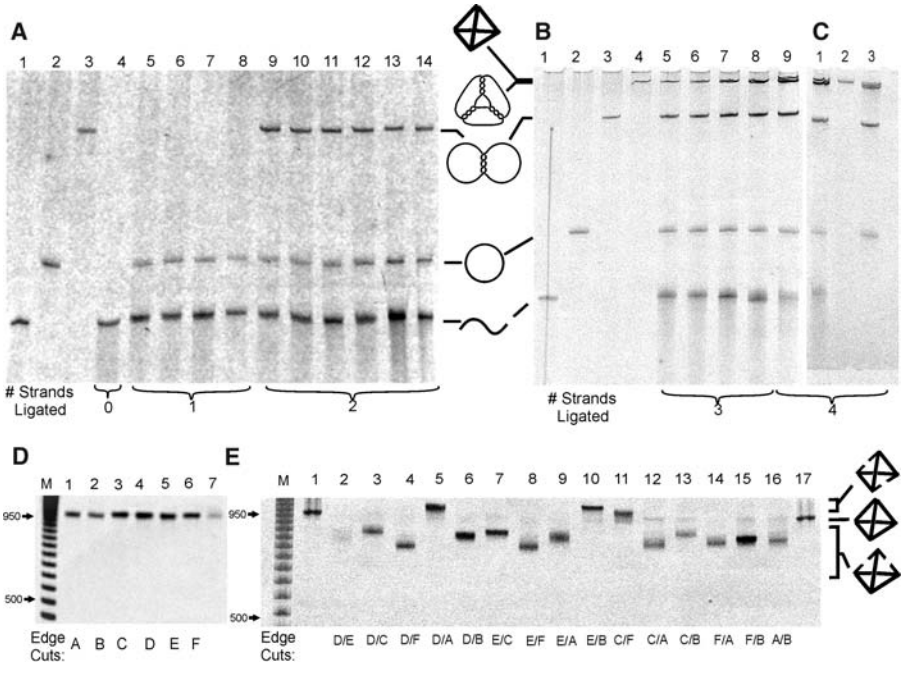

Fig. 2. Topological and structural analysis of a 20-bp regular tetrahedron. (**A** and **B**) Denaturing gels showing products of all possible combinations of ligated and unligated nicks. Control lanes contain oligonucleotides of the same length as the four components of the tetrahedron: linear (lanes A1 and B1), circular (lanes A2 and B2), and double (lanes A3 and B3) and triple (lane B4) linked circles. (**C**) Fully ligated tetrahedron (lane 1) after gel purification (lane 2) and Exo III digestion (lane 3). (**D** and **E**) Edge digestions of a fully ligated tetrahedron on a native gel. (D) Lanes 1 to 6, single cuts; lane 7, uncut tetrahedron. (E) Lanes 2 to 16, double cuts; lanes 1 and 17, uncut tetrahedron. Lane M, 50-bp ladder. See (*13*) for synthesis of markers and for keys to ligated oligonucleotides and edge-cutting enzymes.

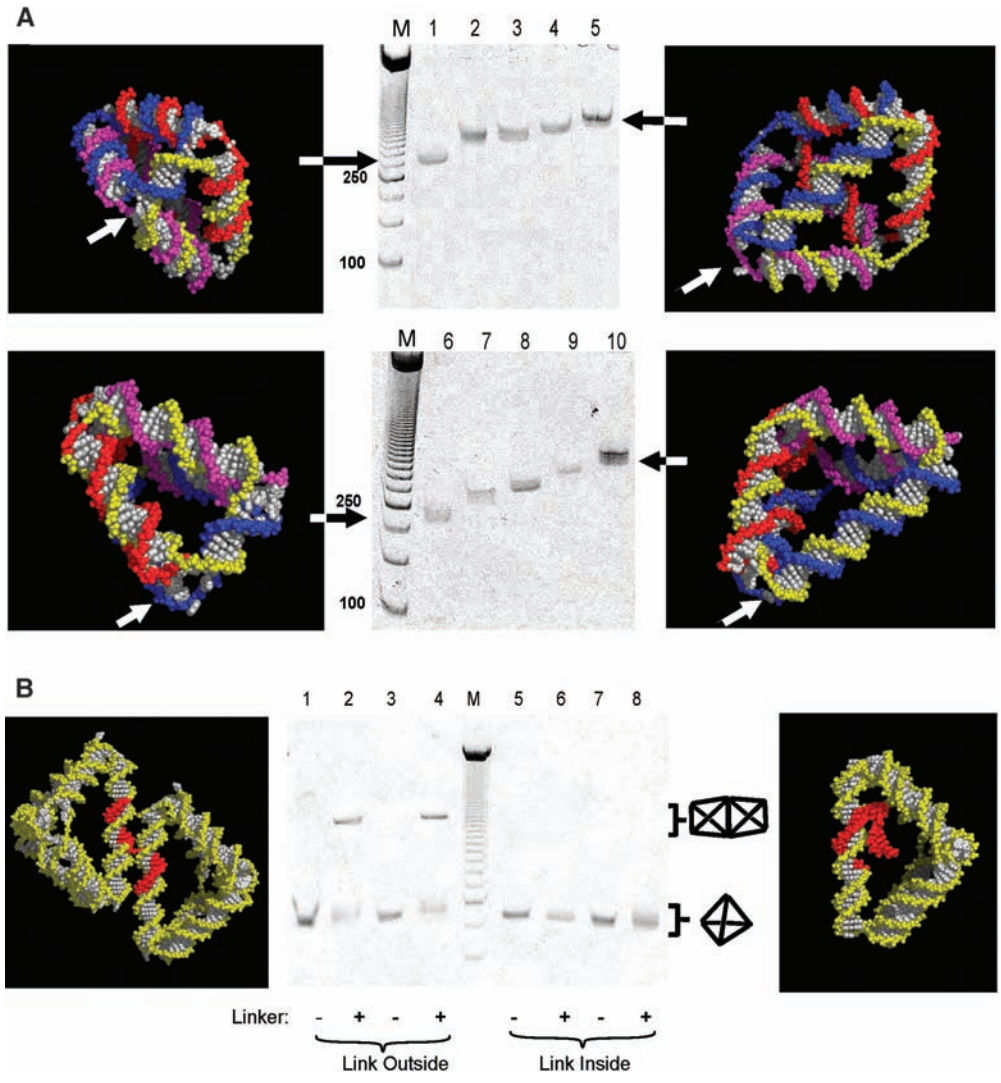

Fig. 3. Versatility and stereoselectivity of tetrahedron synthesis. (**A**) Tetrahedra with five 20-bp edges and one edge of 10 bp (lane 1), 15 bp (lane 2), 20 bp (lane 3), 25 bp (lane 4), or 30 bp (lane 5). Tetrahedra with four 20-bp edges, one 10-bp edge, and an opposite edge of 10 bp (lane 6), 15 bp (lane 7), 20 bp (lane 8), 25 bp (lane 9), or 30 bp (lane 10). For both series the tetrahedra in the first and last lanes are illustrated by 3D models; the edge that is varied is marked with an arrow. (**B**) Linking experiments demonstrating stereoselectivity. A linking strand may join two 5×20/1×30-bp tetrahedra by hybridizing in 10-bp single-stranded gaps in both long edges. There are two possible diastereomers of a DNA tetrahedron. Four gap positions, two in each strand forming the edge, were designed such that the linker would emerge on the outside of one diastereomer, accessible for further hybridization (left panel), and on the inside of the other, hindering further hybridization (right panel). A strong dimer band is observed in only the two cases consistent with the presence of the diastereomer, in which the major groove of each helix faces inward at the vertices. See (*13*) for detailed information on structures. Lane M, 50-bp ladder.

that they contained circular oligonucleotides (Fig. 2C, lane 3). The topology of the corresponding single-, double-, triple-, and quadruple-linked circles can be described using Conway's notation (*14*) as (∞), (–4), (4,4,4), and (6**13.4.13.4.13.4), respectively (fig. S2) (*13*). These results are consistent with the topology of the designed structure.

Because each edge of the tetrahedron has a different base sequence, sequence-specific enzymatic digestion can be used to provide further confirmation of the tetrahedron's tertiary structure. Each edge was designed to contain a different restriction sequence that may be digested (cut) by one of six restriction endonucleases. The effects of edge digestion on a fully ligated tetrahedron are shown using native gels in Fig. 2, D and E. None of the six possible single-edge cuts, not even the blunt cut produced by Alu I (lane 1), had a measurable effect on the tetrahedron's mobility (Fig. 2D). We conclude that the tetrahedron's tertiary structure is particularly stable. The products of each of the 15 possible double-edge digests are shown in Fig. 2E. Three of the cuts created a band with lower mobility than the uncut band; the remaining 12 cut bands had higher mobility. The two groups correspond to two distinct ways of cutting the tetrahedron twice: Higher mobility bands were created by cuts on adjacent edges and lower mobility bands by cuts on opposite edges, confirming the designed relations between edges.

Our assembly method is extremely flexible. Figure 3A shows two series of tetrahedra made with four 20-bp edges; a fifth edge of 20 or 10 bp, respectively; and a sixth edge, opposite the fifth, that varied in length between 10 and 30 bp. Each synthesis resulted in a single-band product whose mobility decreased with increasing edge length. We can also adapt the design to introduce nicks into all six edges (fig. S3) (*13*); single-stranded overhangs at these nicks could be used to create sticky ends to join tetrahedra to make 3D structures.

We have investigated an alternative linking strategy based on the incorporation of a single-stranded gap in a tetrahedron edge (Fig. 3B); oligonucleotides containing two subsequences, each capable of hybridizing in a gap, can be used to link tetrahedra in a programmable manner. A linking strand containing two identical subsequences joins preformed tetrahedra to create homodimers as expected (Fig. 3B, lanes 2 and 4) (fig. S4) (*13*). We have also used linkers incorporating two different binding sequences to create heterodimers (fig. S5) (*13*).

Dimer formation was used to investigate the stereoselectivity of the synthesis. The gapped edge is not free to rotate: The position of the gap along the edge determines the azimuthal position of the free end of the hybridized linker, and thus whether it can reach and hybridize with another tetrahedron. Two gap positions were designed, one for each of the two strands forming the edge, such that the linking strand would project away from the center of one diastereomer but

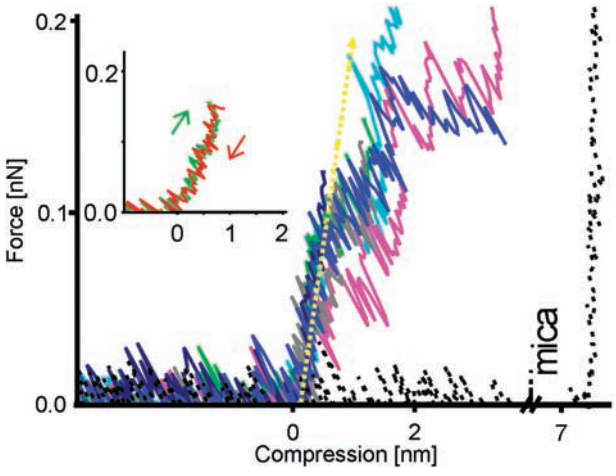

Fig. 4. Compression of single DNA tetrahedra. Compression curves show linear elastic response up to a load of 0.1 nN. At higher forces, most tetrahedra deform irreversibly. Offsets were adjusted to overlap the linear parts of the seven curves. Inset: Reversibility of the elastic response of a typical tetrahedron.

into the center of the other (Fig. 3B, outer panels). In the latter configuration, the linker is expected to be inaccessible. Controls with gaps translated by five bases (half a helical turn) were designed to have the opposite linker orientation. The results of linking experiments for a tetrahedron with 5×20/1×30-bp edges (Fig. 3B) are consistent with the presence of a large excess of the diastereomer in which the major groove of each helix faces inward at each vertex, indicating a significant difference between the formation rates or stabilities of the two possible diastereomers. Stereoselective synthesis, in combination with structural rigidity, ensures that the relative coordinates of any part of the structure can be defined with near-atomic accuracy, an essential property of a nanostructure to be used as a building block for molecular nanofabrication.

We used these structurally braced tetrahedra to investigate the behavior of DNA under compression. Although DNA under tension has been widely studied (*15*–*18*), DNA strands of micrometer length buckle at extremely low forces. Measurement of the response of DNA to large compressive loads could help to resolve the current controversy over the nature of structural changes associated with rare large-angle deformations of the double helix (*19*, *20*). To measure the mechanical response of a single tetrahedron directly, we used an AFM tip as a sensitive force transducer. The tip was centered over a tetrahedron located in imaging mode and was then moved toward the surface while recording force. Compression curves for seven distinct 3×20/3×30-bp tetrahedra, as imaged in Fig. 1, are shown in Fig. 4. For forces up to ~100 pN, the response was approximately linear and reversible (Fig. 4, inset) with an average force constant of 0.18 (±0.07) N m^{-1}. At higher forces, the response was nonlinear and varied from tetrahedron to tetrahedron; tetrahedra generally softened suddenly and deformed irreversibly at a load between 70 and 200 pN.

To model the compressibility of a DNA tetrahedron, we treat its edges as elastic rods pinned (freely hinged) at the vertices. The calculated response of a 3×20/3×30-bp tetrahedron to a compressive load applied between the top vertex and the surface supporting the bottom face is approximately the same for both orientations and is dominated by axial compression of the upstanding edges. The calculated force-displacement (F-d) curve is approximately linear up to a critical load at which the tetrahedron buckles. The boundary conditions at the bottom face have a small effect on the response: If the bottom vertices are not fixed but allowed to slide on the surface, then the bottom edges stretch and the overall stiffness of the construct is reduced by ~3% and ~13% for the tall and short orientations of the tetrahedron, respectively. From the gradient of the linear part of the measured F-d curve, we infer an elastic modulus of K_c = 0.7 (±0.3) nN for one DNA double helix in compression. In the linear response regime, elastic moduli measured by extension and compression should be equal; our value for K_c is near that of the elastic modulus of DNA in tension, K_e ~ 1.1 nN, obtained by fitting the force-extension curves of DNA duplexes (*17*, *18*). Our direct measurement of the axial elastic response of DNA in compression was made possible by the braced structure of the tetrahedron that enabled a short DNA helix to bear a compressive load without bending or tilting.

We can use our measured elastic modulus to estimate the load at which we would expect the edges of a tetrahedron to buckle. If a DNA duplex is modeled as a uniform cylinder of radius r = 1 nm (*21*), then the critical compressive force in an edge at which we would expect Euler instability is $F_c = \pi^2 r^2 K/(2\upsilon l)^2$, where K is the elastic modulus, l is the edge length, and υ is a numerical factor that depends on the boundary conditions at the vertices. If the vertices are pinned, then υ = 1; if the orientations of the edges at the vertices are fixed, then υ = ½. The corresponding AFM tip loads lie in the range from 50 to 300 pN, which is consistent with the range of loads at which tetrahedra were observed to soften suddenly. Our observations of the failure of tetrahedra under high load can thus be explained on the basis of the traditional model of uniform DNA bending (*20*); this result is consistent with our interpretation that the linear part of the F-d curve is caused by pure axial compression of the tetrahedron's upstanding edges before buckling occurs.

The structural changes associated with DNA bending are the subject of controversy. Suggestions that sharp bends due to local melting or kinking (*22*) are observed in DNA cyclization experiments (*19*, *23*, *24*) are countered by measurements that indicate that the probability of such kinks is very low (*20*). Extended observation of tetrahedra under compression may be a useful method for investigating the energy and sequence dependence of inhomogeneous bending and of the effects of compressive strain on DNA-protein interactions.

References and Notes

1. N. C. Seeman, *Nature* **421**, 427 (2003).
2. Commercial oligonucleotide synthesis costs ~50¢ per base for several nanomoles and, at its simplest, fabrication requires only mixing of aqueous solutions.
3. E. Winfree, F. R. Liu, L. A. Wenzler, N. C. Seeman, *Nature* **394**, 539 (1998).
4. J. Malo *et al.*, *Angew. Chem. Int. Ed.* **44**, 3057 (2005).
5. H. Yan, S. H. Park, G. Finkelstein, J. H. Reif, T. H. LaBean, *Science* **301**, 1882 (2003).
6. J. H. Chen, N. C. Seeman, *Nature* **350**, 631 (1991).
7. Y. W. Zhang, N. C. Seeman, *J. Am. Chem. Soc.* **116**, 1661 (1994).
8. W. M. Shih, J. D. Quispe, G. F. Joyce, *Nature* **427**, 618 (2004).
9. M. Scheffler, A. Dorenbeck, S. Jordan, M. Wüstefeld, G. von Kiedrowski, *Angew. Chem. Int. Ed.* **38**, 3312 (1999).
10. A. Dorenbeck, thesis, Ruhr-Universität Bochum (2000).
11. X. Zhang, H. Yan, Z. Y. Shen, N. C. Seeman, *J. Am. Chem. Soc.* **124**, 12940 (2002).
12. In a preliminary communication (*25*), we introduced a tetrahedral nanostructure with nicks positioned such that helices could separate and unwind at the vertices; this construct was not expected to resist deformation.
13. See supporting data on *Science* Online.
14. J. H. Conway, in *Computation Problems in Abstract Algebra*, J. Leech, Ed. (Pergamon, Oxford, 1970).
15. C. Bustamante, J. F. Marko, E. D. Siggia, S. Smith, *Science* **265**, 1599 (1994).
16. S. B. Smith, Y. Cui, C. Bustamante, *Science* **271**, 795 (1996).
17. M. D. Wang, H. Yin, R. Landick, J. Gelles, S. M. Block, *Biophys. J.* **72**, 1335 (1997).
18. C. G. Baumann, S. B. Smith, V. A. Bloomfield, C. Bustamante, *Proc. Natl. Acad. Sci. U.S.A.* **94**, 6185 (1997).
19. T. E. Cloutier, J. Widom, *Proc. Natl. Acad. Sci. U.S.A.* **102**, 3645 (2005).
20. Q. Du, C. Smith, N. Shiffeldrim, M. Vologodskaia, A. Vologodskii, *Proc. Natl. Acad. Sci. U.S.A.* **102**, 5397 (2005).
21. M. E. Hogan, R. H. Austin, *Nature* **329**, 263 (1987).
22. F. H. C. Crick, A. Klug, *Nature* **255**, 530 (1975).
23. J. Yan, J. F. Marko, *Phys. Rev. Lett.* **93**, 108108 (2004).
24. P. A. Wiggins, R. Phillips, P. C. Nelson, *Phys. Rev. E* **71**, 021909 (2005).

25. R. P. Goodman, R. M. Berry, A. J. Turberfield, *Chem. Commun.* **2004**, 1372 (2004).
26. We thank J. Johannes for advice on the topology of circular catenanes. Supported by the UK Biotechnology and Biological Sciences Research Council, Engineering and Physical Sciences Research Council, Medical Research Council, and Ministry of Defence (through the UK Bionanotechnology Interdisciplinary Research Collaboration); the Oxford Life Sciences Interface Doctoral Training Centre; the Rhodes Trust; the Natural Sciences and Engineering Research Council of Canada; and the Foundation for Fundamental Research on Matter (FOM).

Supporting Online Material
www.sciencemag.org/cgi/content/full/310/5754/1661/DC1
Materials and Methods
SOM Text
Figs. S1 to S5
References

20 September 2005; accepted 7 November 2005
10.1126/science.1120367

The Chemistry of Deformation: How Solutes Soften Pure Metals

Dallas R. Trinkle* and Christopher Woodward

Solutes have been added to strengthen elemental metals, generating usable materials for millennia; in the 1960s, solutes were found to also soften metals. Despite the empirical correlation between the "electron number" of the solute and the change in strength of the material to which it is added, the mechanism responsible for softening is poorly understood. Using state-of-the-art quantum-mechanical methods, we studied the direct interaction of transition-metal solutes with dislocations in molybdenum. The interaction increases dramatically with increasing electron number and strongly influences the mechanisms responsible for plasticity in these materials. Our quantitative model explains solution softening of metals by using changes in energy and stress scales of plasticity from solutes.

Solutes have played a key role in producing useful materials from pure metals over the past millennia, driving technological advances in civilization—from the Bronze Age to the Iron Age to the industrial revolution. For most of human history, alloying was used to increase the strength of metals (*1*). Four decades ago, a wealth of evidence showed that for some body-centered cubic (bcc) metals, solutes could decrease material strength (*2*). This effect, known as solid-solution softening, was observed as a reduction in the stress at which a material begins to deform irreversibly (yield stress) or as a reduction in the material's ability to resist indentation (hardness). Softening is important for producing viable materials: The bcc refractory metals (Nb, W, Ta, and Mo) offer a possible new class of high-temperature materials for components used in turbine engines or nuclear power plants, but the metals have poor low-temperature behavior in elemental form. As the temperature decreases from 15% of the melting temperature (above room temperature for refractory metals) down to absolute zero, strength increases rapidly. This high strength is undesirable, because it is linked with an increase in fracture and low malleability, ultimately limiting the use of these materials as critical structural components. A classical metallurgical practice is to reduce this risk by incorporating solid-solutions or by introducing new softer phases. Models have only succeeded in qualitatively explaining the possibility of low-temperature softening (*3*–*5*) or in finding empirical correlations to deduce scaling trends (*6*). Moving beyond these empirical techniques requires a combination of chemistry, materials physics, and large-scale computation to investigate how solute chemistry changes deformation: the "chemistry of deformation."

Irreversible plastic deformation of metals is controlled by dislocation defects, and solute-induced softening is controlled by interactions of solutes and dislocations. Dislocations are topological line defects that move at stresses below the stress required to irreversibly deform a dislocation-free crystal (*7*). In bcc metals, low-temperature plastic deformation is controlled by moving straight screw-character dislocations. A dislocation line moves perpendicular to its length by nucleating a pair of opposite-directed "kinks." These migrate away from each other along the dislocation, moving the dislocation line forward to the next lattice site like the locomotion of a snake. Solute chemistry affects double-kink nucleation and kink migration to produce both softening and hardening.

Our model explains the following experimental data for a Mo-Re alloy, which is the classic solid-solution softening system. Below a temperature of 350 K, Mo-Re is softer than pure Mo for small Re concentrations (*8*). Softening continues up to 16 atomic %, where the alloy becomes harder than pure Mo. The maximum softening occurs at 8 atomic % at 77 K, and the maximum softening concentration decreases as temperature is increased (*9*). Thus, a given solute concentration can soften an alloy at one temperature and harden at another; and at a given temperature, increasing solute concentration can first soften and then harden the alloy at higher concentrations. Similar features appear for other 5d-row solutes with higher d electron numbers (Os, Ir, Pt), but the maximum softening occurs at much smaller concentrations. Metals with lower d electron numbers (Hf, Ta) harden for all concentrations and temperatures. The goal of alloy design for Mo alloys is to soften the low-temperature behavior, reducing the risk of fracture.

We show here that the prediction of strength with changing alloy concentration and temperature for Mo alloys requires calculation of the direct solute-dislocation interaction and modeling of those effects on plasticity. State-of-the-art quantum-mechanical electronic structure methods (*10*–*13*) with special dislocation boundary conditions (*14*) calculate the interaction energy between a single straight dislocation and a solute and the change in the resistance to the motion of the dislocation. These data enter a solid-solution softening model of plasticity by changing energy and stress scales of double-kink nucleation and kink-migration enthalpy barriers. The effect of random clustering (where more than one solute atom interacts with a kink) is crucial in modeling changes in kink migration above the dilute limit. Also, the bonding environment near a dislocation is distinct from the bulk, producing the unique chemistry of deformation. Our model quantitatively predicts strength measurements of Mo-Re and matches hardness measurements of Mo-Pt, two systems with dramatically different softening and hardening behavior. The details of the computational methods are included in (*15*).

As a starting point, Fig. 1 compares the nearest-neighbor geometry of bulk bcc Mo to that of a 1/2[111] screw-character dislocation. Viewed along the [111] direction, the bulk cubic structure forms a triangular lattice of atomic rows; the triangles can be viewed as spirals of alternating chirality. To form a dislocation, the chirality of a triangle is changed by displacing each row in the triangle by different amounts

Materials and Manufacturing Directorate, Air Force Research Laboratory, Wright Patterson Air Force Base, Dayton, OH 45433–7817, USA.

*To whom correspondence should be addressed. E-mail: dallas.trinkle@wpafb.af.mil